Preliminary design of a small-sized flapping UAV. II. Aerodynamic Performance and Flight Stability

Joel E. Guerrero[1], Carlo Pacioselli[1], Jan Oscar Pralits[1], Francesca Negrello[1], Paolo Silvestri[2], Alessandro Bottaro[1]

[1]*Department of Civil, Chemical and Environmental Engineering, University of Genova, Italy*
E-mail: alessandro.bottaro@unige.it

[2]*Department of Mechanical Engineering, University of Genova, Italy*
E-mail: p.silvestri@unige.it

SUMMARY. In this work, we present the preliminary design of a biologically inspired flapping UAV. Starting from a set of initial design specifications, namely: weight, maximum flapping frequency and the minimum hand-launch velocity of the model; we conduct a wide numerical study of the proposed avian model in terms of the aerodynamic performance and flight stability in flapping and gliding conditions. The model shape, size and flight conditions are chosen to approximate those of a seagull. Additionally, an extensive study is conducted in order to dissect the kinematics of the wings, where starting from the simplest wing kinematics we keep on adding more degrees of freedom and control parameters until reaching a functional and realistic wing kinematics. The results give us an initial insight of the aerodynamic performance and flight stability of a biomimetic flapping UAV designed at minimum flight velocity and maximum flapping frequency.

1 INTRODUCTION

In conventional man-made flying vehicles the wings provide the lift and the engines provide the thrust. In a bird, however, the wings have to provide the thrust as well as the lift, with the added complication that they are used to maneuver as well. Birds are amazing examples of unsteady aerodynamics, high maneuverability, endurance, flight stability and control, and large aerodynamic efficiency; birds are the result of million of years of evolution. Despite the progress made during the past years in the area of the unsteady aerodynamics and flight dynamics of birds flight, control systems, materials science and robotics and automation [1]-[9], designing a biomimetic autonomous flapping unmanned aerial vehicle (UAV) is the ultimate design challenge for engineers and scientists.

In this manuscript, we present the preliminary design of a biologically inspired small-sized flapping UAV. Flapping UAVs and flapping micro-air-vehicles (MAVs), capable of flying like birds or insects and operating in the same range of velocities as they do, and being able to show the same morphology and camouflage as their biological counterparts, will fill the space left void by conventional fixed wing and rotary wings UAVs and MAVs in terms of maneuverability and aerodynamic efficiency when operating at low Reynolds numbers [10, 11]. This manuscript summarizes some key technical issues of a flapping UAV, where the shape and size of the model were chosen in terms of the morphology of several birds, and in order to prove the concept we numerically simulated the proposed avian model in flapping and gliding flight.

2 DESIGN SPECIFICATIONS AND AVIAN MODEL DESIGN APPROXIMATIONS

In table 1, we present the design specifications for the proposed flapping UAV. One important design specification to highlight is that the vehicle is intended to be hand launched with a minimum

velocity of 5.0 m/s. It is also interesting to point out that the flapping frequency can be modulated, but shall not exceed 3.0 Hz, this constraint is imposed for structural reasons. Hereafter, we enumerate a few design approximations used during this study,

- The avian model is treated as a rigid body to simplify the equations that describe the dynamics.

- For the flapping flight simulations, the wings are considered to be made of two parts, one internal wing and one external wing, with a gap between the internal and external wings. This gap is where the wing is considered to be articulated.

- The junction between the wing and the body of the avian model is also modeled through a gap.

- The mass of the avian model is assumed to be distributed uniformly.

- The fuselage is assumed to have a light shell making it look like a bird. This shell generates drag and lift, which are taken into account for the aerodynamic forces computations.

Table 1: Design specifications.

Maximum weight	1.0 kg
Maximum flapping frequency	3.0 Hz
Minimum velocity (hand launch velocity)	5.0 m/s
Maximum velocity	14.0 m/s
Autonomy	20.0 min

3   AVIAN MODEL AND REFERENCE GEOMETRY

Taking into account the design specifications and morphometrics/allometry of several birds [12, 13, 14], we proceed to determine the initial form of the avian model. The model shape, size, and flight conditions were chosen to approximate those of a seagull (Kelp Gull or Western Gull), which closely meets our design specifications. In table 2 we show the geometric data of the proposed avian model.

Table 2: Avian model geometric data.

Wing projected area S_w (one wing)	0.314 m^2
Wing mean aerodynamic chord MAC_w	0.336 m
Wing semi-span b	1.0 m
Tail projected area (half the tail) S_h	0.087 m^2
Tail mean aerodynamic chord MAC_h	0.444 m
Fuselage maximum diameter	0.2 m
Fuselage length	1.0 m
Fuselage projected area (half the fuselage) S_f	0.066 m^2

The wing used in this study is a simplification of the actual wing of a seagull obtained by Liu *et. al* [15], where they extracted the wing surface coordinates by using a 3D laser scanner. The

simplified or engineered wing was used in order to parametrize the 3D model and to avoid potential surface modeling problems when conducting the parametric study. The wing dimensions were chosen in such a way that they produce the lift needed to keep the avian model aloft at the design conditions of a forward velocity of 5.0 m/s and a flapping frequency of 3.0 Hz, that is, the model is designed at minimum flight velocity and maximum flapping frequency.

The fuselage is designed in such a way that it provides enough room to house the mechanisms and flight systems with no interference, it produces low drag, it has a low negative contribution to the overall stability of the model and resembles a seagull. Finally, an horizontal stabilizer or tail was added to the model and it was sized in such a way that it guarantees the stability of the avian model in flapping and gliding flight. It is important to mention that the whole tail is allowed to move.

In figure 1, we present an illustration of the avian model. In this figure, the point marked as 000 represents the junction between the fuselage and the internal wing and also serves as a reference point to define the wing kinematics, the position of the different components of the avian model, the position of the aerodynamic center of the wing and tail and the position of the center of gravity of the model. The axis 100 (which passes through the point 000), is the axis about which the internal wing oscillates or rolls, and the axis 200 is the axis about which the external wing is articulated and rolls.
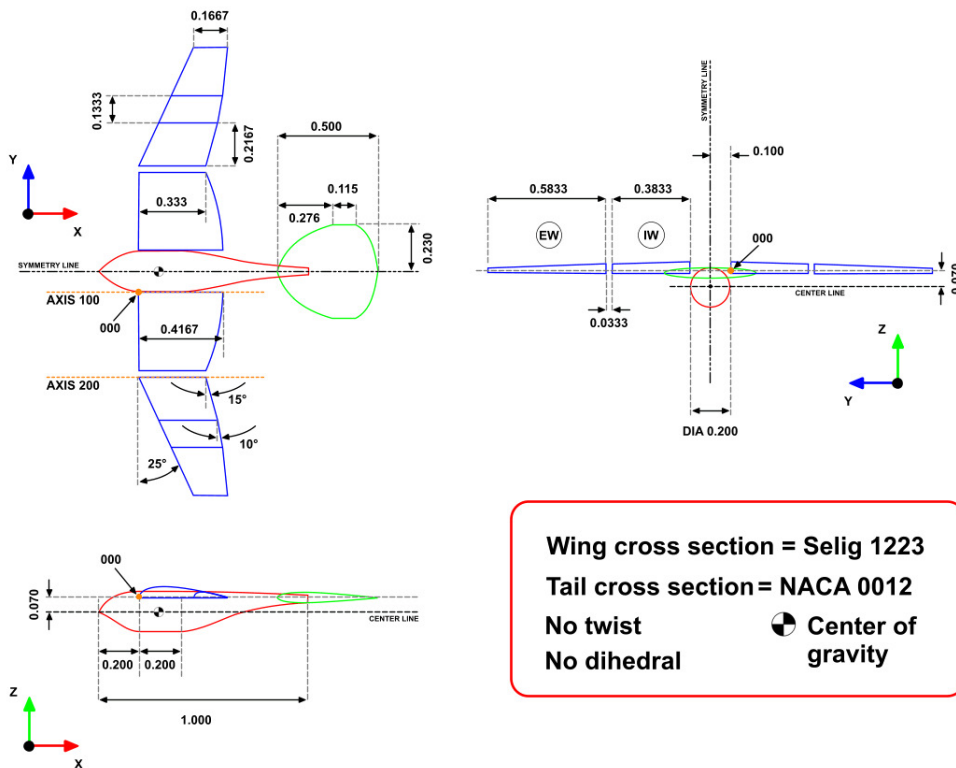
Figure 1: Three-view of the avian model. EW stands for external wing, and IW stands for internal wing. All dimensions are in meters.

3

4   WING KINEMATICS

Birds and insects wings follow complex patterns, which often involve rotation and translation with several degrees of freedom and even deformation. However, for the sake of simplicity, we represent the flapping motion as the rolling motion of the internal wing about the axis 100 and the rolling motion of the external wing about the axis 200 (see figure 1). The equations that describe this motion are as follows,

$$roll_{iw} = A_{iw} \times sin(\omega \times t), \tag{1}$$

$$droll_{iw} = \omega \times A_{iw} \times cos(\omega \times t), \tag{2}$$

$$roll_{ew} = -\frac{A_{ie} \times \frac{\pi}{2} \times erf(\sqrt{2} \times \sqrt{B} \times cos(\omega \times t))}{2 \times \sqrt{B} \times C}, \tag{3}$$

$$droll_{ew} = \frac{A_{ie} \times \omega \times sin(\omega \times t) \times e^{(B \times sin(2 \times \omega \times t - \frac{\pi}{2}) - B)}}{C}; \tag{4}$$

where $roll$ is the roll angle of the wing (measured in °) and $droll$ is the angular velocity of the wing (measured in °/s), the subscript iw stands for internal wing, the subscript ew stands for external wing, A_{iw} is the maximum roll amplitude of the internal wing, A_{ie} is the maximum angle between the internal wing and external wing, ω is the angular frequency ($2\pi f$), f is the flapping frequency, t is the time and erf is the error function ($erf(x) = \frac{2}{\sqrt{\pi}} \int_0^x e^{-t^2} dt$). In equations 1-2, the amplitude A_{iw} is equal to 30°; in equations 3-4 the amplitude A_{ie} is equal to 50°, and the constants B and C are equal to 1.0 and 1.1963 respectively. The flapping frequency is equal to 3.0 Hz.

In figures 2 and 3, we show the time evolution of the roll angle and the angular velocity respectively, for both the internal and the external wings. The kinematics was designed in such a way that it generates the required lift and it produces thrust at the design conditions of forward velocity equal to 5.0 m/s and flapping frequency equal to 3.0 Hz. Additionally, we carefully adjusted the kinematics in order to have the internal and external wings aligned as much as possible during the downstroke (refer to figure 2), not to generate high angular velocities when the external wing begins to rotate when it approaches the end of the downstroke and upstroke (refer to figure 3). The aim is to have a kinematics that resembles the flapping motion of actual birds.

In addition to equations 1-4, the following equations are needed to track the spatial position of the articulation axis 200,

$$z_{iw} = 1.0 \times (l_{int} + l_{gap}) \times cos(roll_{iw}), \tag{5}$$

$$y_{iw} = -1.0 \times (l_{int} + l_{gap}) \times sin(roll_{iw}), \tag{6}$$

$$dz_{iw} = -1.0 \times (l_{int} + l_{gap}) \times sin(roll_{iw}) \times droll_{iw}, \tag{7}$$

$$dy_{iw} = -1.0 \times (l_{int} + l_{gap}) \times cos(roll_{iw}) \times droll_{iw}. \tag{8}$$

Equations 5 and 6, tracks the position in the z axis and y axis of the points located at a distance equal to the length of the internal wing or l_{int} plus the length of the gap between the wings or l_{gap};

4
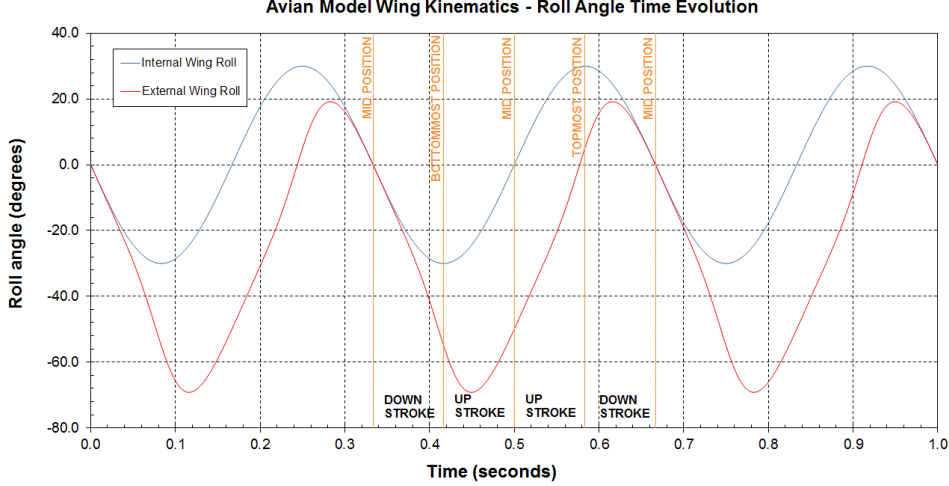
Figure 2: Time evolution of the roll angle. The vertical orange lines represent different instants during one flapping period.

where $l_{int} = 0.3833\ m$ and $l_{gap} = 0.0333\ m$. This distance is measured with reference to the point 000 (refer to figure 1). Equations 7-8 are used to obtain the linear velocities dz and dy along the z axis and y axis, respectively.

Finally, to track the spatial position and compute the linear velocities of the external wing in the direction of the axis z and y, equations 9-12 are used. These equations are expressed in terms of the reference length l_{cg}, which for our case is equal to the distance of the center of gravity of the external wing with respect to the axis 200 or $l_{cg} = 0.2333\ m$.

$$z_{ew} = 1.0 \times (l_{cg}) \times (roll_{iw} + roll_{ew}), \tag{9}$$

$$y_{ew} = -1.0 \times (l_{cg}) \times sin(roll_{iw} + roll_{ew}), \tag{10}$$

$$dz_{ew} = -1.0 \times (l_{cg}) \times sin(roll_{iw} + roll_{ew}) \times (droll_{iw} + droll_{ew}), \tag{11}$$

$$dy_{ew} = -1.0 \times (l_{cg}) \times cos(roll_{iw} + roll_{ew}) \times (droll_{iw} + droll_{ew}). \tag{12}$$

5   AERODYNAMIC PERFORMANCE IN GLIDING AND FLAPPING FLIGHT

In this study, the unsteady incompressible Reynolds-Averaged Navier-Stokes (URANS) equations are solved by using the commercial finite volume solver Ansys® Fluent [16]. The cell-centered values of the computed variables are interpolated at the face locations using a second-order centered difference scheme for the diffusion terms. The convective terms at cell faces are interpolated by means of a second-order upwind scheme. For computing the gradients at cell-centers, the least squares cell-based reconstruction method is used. In order to prevent spurious oscillations a multidimensional slope limiter is used, which enforce the monotonicity principle by prohibiting the linearly

5
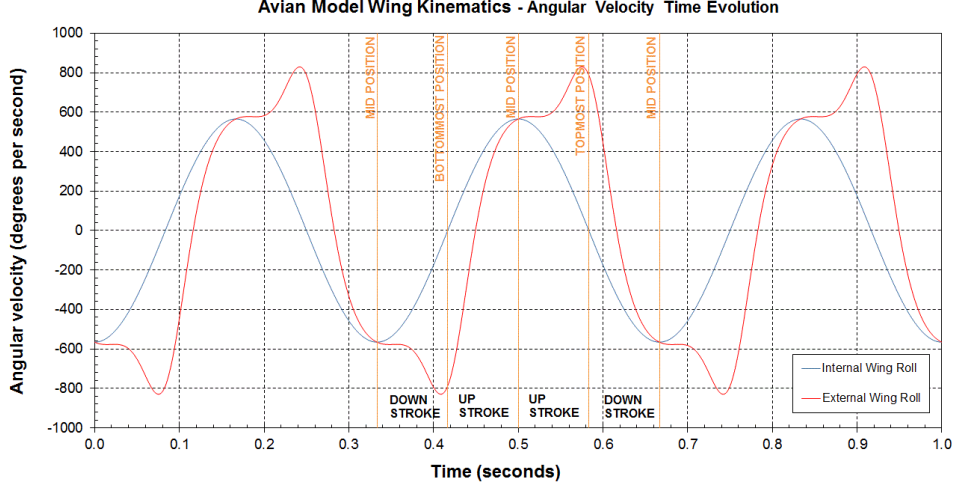
Figure 3: Time evolution of the angular velocity. The vertical orange lines represent different instants during one flapping period.

reconstructed field variables on the cell faces to exceed the maximum or minimum of the neighboring cells. This results in a total variation diminishing (TVD) scheme that guarantees the accuracy, stability and boundedness of the solution. The pressure-velocity coupling is achieved by means of the PISO algorithm and as the solution takes place in collocated meshes, the Rhie-Chow interpolation scheme is used to prevent the pressure checkerboard instability. For turbulence modeling, the shear-stress transport (SST) $\kappa - \omega$ model is used with wall functions. The turbulence quantities, turbulent kinetic energy κ and specific dissipation rate ω, are discretized using the same scheme as for the convective terms. To handle the moving bodies, the dynamic meshing model was employed [16], where we used mesh diffusion smoothing; in order to avoid degenerated cells remeshing was used every two time steps. The time-step was chosen in such a way that the CFL number is not greater than 0.9.

The lift force L and drag force D are calculated by integrating the pressure and wall-shear stresses over the surface of the avian model; then, the lift coefficient C_L and drag coefficient C_D are computed as follows,

$$C_L = \frac{L}{0.5 \times \rho \times V_\infty^2 \times S_{ref}} \quad ; \quad C_D = \frac{D}{0.5 \times \rho \times V_\infty^2 \times S_{ref}}, \tag{13}$$

where ρ is the air density ($\rho = 1.225\,kg/m^3$), V_∞ is the forward velocity (measured in m/s), and S_{ref} is the reference area used to compute the non-dimensional coefficients ($S_{ref} = 0.314\,m^2$). As for the lift and drag forces, the moment is computed by integrating the pressure and wall-shear stresses over the surface of the model and about the center of gravity CG1. Then, the pitching moment coefficient is computed as follows,

$$C_M = \frac{M}{0.5 \times \rho \times V_\infty^2 \times S_{ref} \times c} \tag{14}$$

6

where c is the mean aerodynamic chord of the wing or MAC_w. As we are dealing with an unsteady aerodynamics case, *i.e.*, the wings are flapping, the lift, drag and moment coefficients are averaged in time as follows,

$$\overline{C}_L = \frac{1}{\mathbb{T}} \int_t^{t+\mathbb{T}} C_L(t)dt \;\; ; \;\; \overline{C}_D = \frac{1}{\mathbb{T}} \int_t^{t+\mathbb{T}} C_D(t) \;\; ; \;\; \overline{C}_M = \frac{1}{\mathbb{T}} \int_t^{t+\mathbb{T}} C_M(t) \quad (15)$$

where $\mathbb{T}$ is the period of the flapping motion ($\mathbb{T} = 1/f$). All coefficient were averaged over the fourth period of the oscillations.

In figure 4, we present the drag polar of the avian model in flapping flight. As at this point we are not interested in the stability of the avian model, the results shown are for the model configuration with no tail. As it can be seen in this figure, the avian model is able to produce thrust in the flight envelope explored (in the figure, negative drag coefficient means thrust production). We can also observe that we meet the design requirement of minimum velocity of 5.0 m/s and maximum flapping frequency of 3.0 Hz. This design condition is obtained at $0°$ pitch angle. In the figure, positive values of pitch angle means nose-up attitude, whereas negative values are an indication of nose-down attitude.
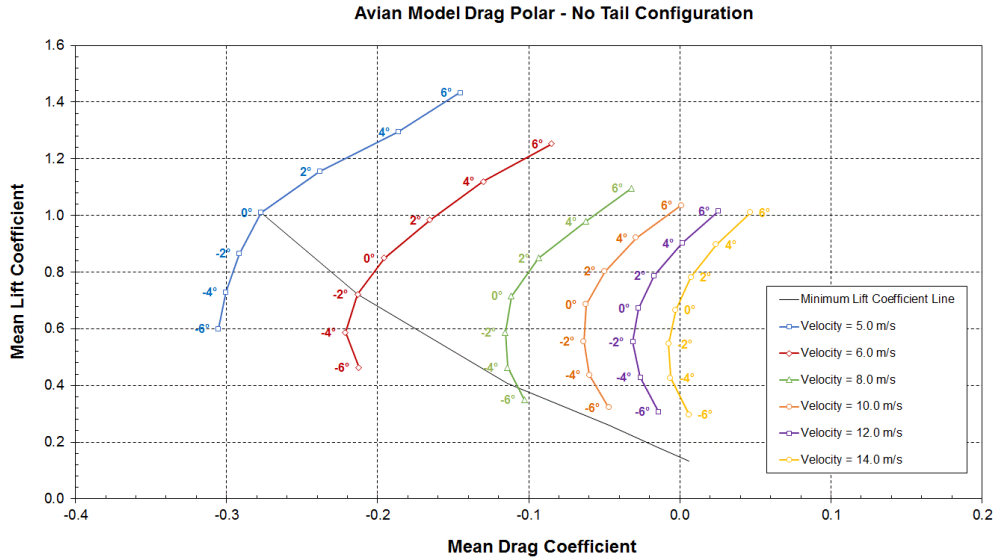
Figure 4: Drag polar for the no tail configuration. The numbers next to the curves, indicate the pitch angle of the avian model.

6 STATIC STABILITY IN GLIDING AND FLAPPING FLIGHT

For computing the static stability of the avian model, we first need to define the position of the center of gravity CG1 about which the moment is computed. With reference to point 000, CG1 is located 0.094 m in the x direction, 0.1 m in the y direction, and -0.074 m in the z direction or 28% of the MAC_w. Before discussing the stability in flapping flight, we need to study first the stability

in gliding flight. The results shown in figure 5, correspond to a configuration of the avian model with the tail deflected by 15° degrees, where a positive tail deflection indicates that it produces a pitch-up attitude in the model. The tail hinges about the rearmost fuselage part, *i.e.* $x = 0.685\ m$. As it can be observed in this figure, the model has a positive trim angle about a pitch angle value of approximately $0°$. Also, the slope of the pitching moment coefficient curve is negative, which is an indication of positive stability.

Let us now study the case for flapping flight. In figures 6 and 7, we show the results for the avian model with the tail deflected at $20°$ and $15°$, respectively. By examining both figures, we can highlight that the avian model has positive stability and a trim point within the flight envelope. For the case of tail deflection equal to $20°$ and forward velocity equal to $5.0\ m/s$ (see figure 6), the avian model has a trim point close to zero; for the case of tail deflection equal to $15°$ and forward velocity equal to $5.0\ m/s$ (see figure 7), the trim point is approximately equal to -3.0°. These results clearly illustrate that the model is stable, trimmable and controllable within the limits of the flight envelope and the tail deflection angles studied. Similar observations apply to all velocity values explored, with the caveat that at higher velocities and same pitch angle the lift force and moment about CG1 are higher, hence the trim angle increases.
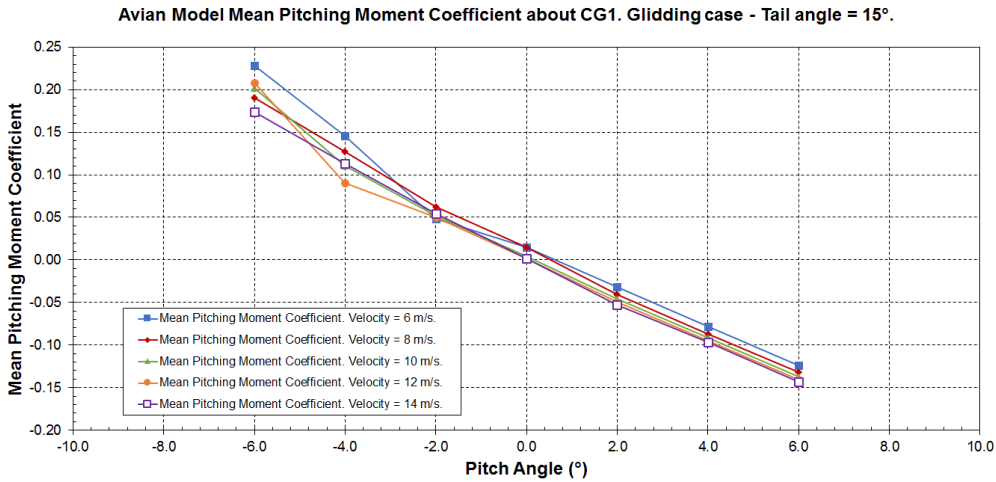
Figure 5: Gliding case mean pitching moment coefficient about CG1. Tail deflection equals $15°$.

7   CONCLUSIONS AND PERSPECTIVES

In this manuscript, we have presented a few results on the aerodynamic performance and static stability of a biomimetic flapping UAV. For the design goals and the wide range of velocities, pitch angles and tail deflection angles studied, it was found that the avian model and kinematics proposed were able to fulfill the design requirements. For the flight envelope studied, the avian model is able to produce thrust up to a velocity of approximately $14.0\ m/s$ and it generates enough lift to meet and exceed the weight constrains. It was also found that for the tail sizing and tail deflection angles considered the model has positive stability and it is trimmable in flapping and gliding flight, leaving a good margin of controllability. Additionally, we were able to obtain a kinematics that

Avian Model Mean Pitching Moment Coefficient about CG1. Flapping case - Tail angle = 20°.
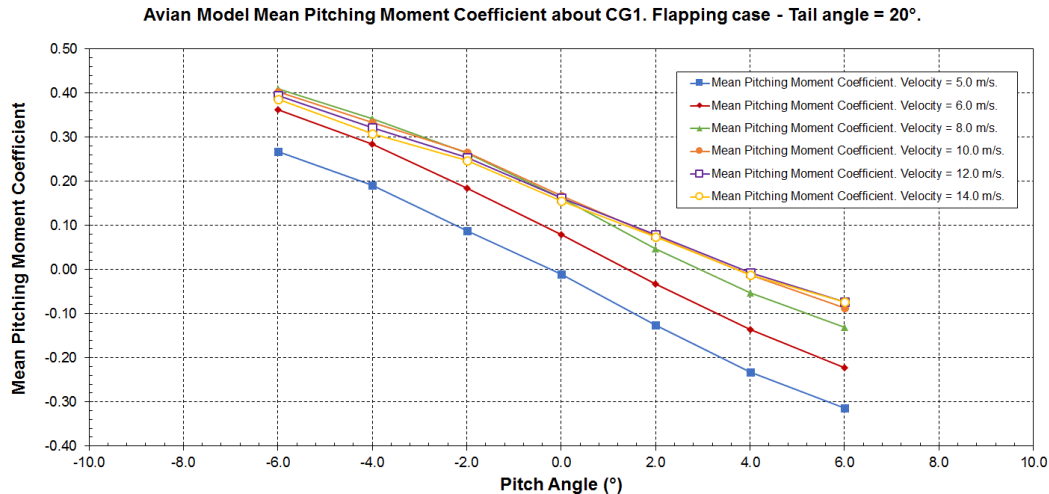
Figure 6: Flapping case mean pitching moment coefficient about CG1. Tail deflection equals $20°$.

approximates that of birds and, by carefully adjusting the kinematics parameters, we managed to avoid high angular velocities and inertial loads that could compromise the structural integrity or destabilize the avian model.

It is envisaged in the future the extension of the current study to lateral stability in flapping and gliding flight, dynamic stability in flapping flight by using a multibody dynamics approach and the design of a control system.

References

[1] Prosser, D., Basrai, T., Dickert, J., Ratti, J., Crassidis, A., Vachtsevanos, G., "Wing kinematics and aerodynamics of a hovering flapping Micro Aerial Vehicle ," Aerospace Conference, 2011 IEEE, pp. 1-10, 5-12 March, 2011.

[2] Wen, X., Gang, S., "Airfoil design and aerodynamic force testing for flapping-wing Micro Air Vehicles," Intelligent Control and Automation, 2012 10th World Congress on, pp. 3933-3938, 6-8 July, 2012.

[3] Maeng, JS., Park JH., Jang SM., Han SY., "A modeling approach to energy savings of flying Canada geese using computational fluid dynamics," Journal of Theoretical Biology, **320**, pp. 76-85, 2013.

[4] Hubel, T., Tropea, C., "Experimental investigation of a flapping wing model," Experiments in Fluids, **46**, Issue 5, pp. 945-961, 2009.

[5] Parslew, B., Crowther, W., "Simulating avian wingbeat kinematics," Journal of Biomechanics, **43**, pp. 3191-3198, 2010.

[6] Nakata, T., Liu, H., Tanaka, Y., Nishihashi, N., Wang, X., Sato, A., "Aerodynamics of a bio-inspired flexible flapping-wing micro air vehicle," Bioinspiration & Biomimetics, **6**, 045002, 11pp, 2011.

Avian Model Mean Pitching Moment Coefficient about CG1. Flapping case - Tail angle = 15°.
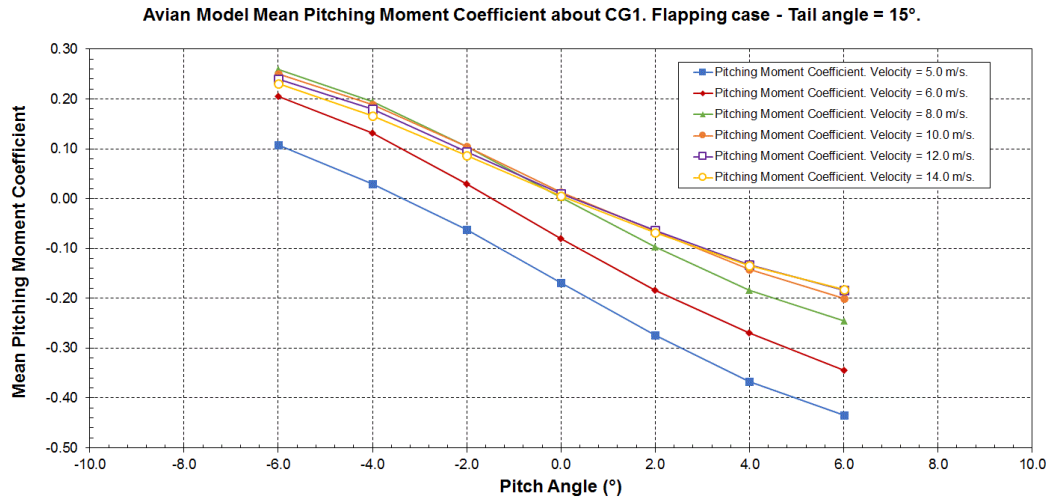
Figure 7: Flapping case mean pitching moment coefficient about CG1. Tail deflection equals $15°$.

[7] Tsai, B., Fu, YC., "Design and aerodynamic analysis of a flapping-wing micro aerial vehicle," Aerospace Science and Technology, **13**, pp. 383-392, 2009.

[8] Thomas, A., Taylor, G., "Animal Flight Dynamics I. Stability in Gliding Flight," Journal of Theoretical Biology, **212**, pp. 399-424, 2001.

[9] Thomas, A., Taylor, G., "Animal Flight Dynamics II. Longitudinal Stability in Flapping Flight," Journal of Theoretical Biology, **214**, pp. 351-370, 2002.

[10] Mueller, T., DeLaurier, J. , "Aerodynamics of small vehicles ," Annual Review of Fluid Mechanics, **35**, pp. 89-111, 2003.

[11] Shyy, W., Lian, Y., Tang, J., Viieru, Dragos., Liu, Hao., *"Aerodynamics of Low Reynolds Number Flyers* ," Cambridge Aerospace Series. 2007.

[12] Bruderer, B., Boldt, A., "Flight characteristics of birds: I. radar measurements of speeds," IBIS The International Journal of avian science, **143**, Issue 2, pp. 178-204, 2001.

[13] Bruderer, B., Peter, D., Boldt, A., Liechti, F., "Wing-beat characteristics of birds recorded with tracking radar and cine camera" IBIS The International Journal of avian science, **152**, Issue 2, pp. 272-291, 2010.

[14] Pennycuick, C., *"Modelling the Flying Bird,"* Elsevier, 2008.

[15] Liu, T., Kuykendoll, K., Rhew, R., Jones, S., "Avian Wings," 24th AIAA Aerodynamic Measurement Technology and Ground Testing Conference, AIAA 2004-2186, Portland, 2004.

[16] Ansys® Academic Research, Release 14, Help System, Ansys Fluent Theory Guide, ANSYS, Inc.